METHODS FOR ESTIMATING APPARENT DENSITY OF SEDIMENT IN SUSPENSION USING OPTICS

by

Alexander Hurley

Submitted in partial fulfillment of the requirements for the
degree of Master of Science

at

Dalhousie University
Halifax, Nova Scotia
April 2015

Table of Contents

List of Tables

List of Figures

Abstract

In most aquatic environments, suspended sediment is composed of loosely packed particle aggregates, termed flocs, that have variable apparent densities. The apparent density of flocs, which is defined as particle dry mass over wet volume, is an important variable because it affects vertical sediment flux and light scattering per unit mass in the ocean. Two established methods exist for measuring apparent density. One method uses physical measurements of sediment mass combined with measurements of particle volume from optical instruments to estimate apparent density. This method is laborious because it requires the collection of water samples and is not conducive to construction of high resolution time series of density. Another method uses video observations of particles in a settling column to measure particle size and settling velocity. These measurements are used to solve for apparent density according to Stokes Law. The goal of this study is to compare a new method that uses the ratio of particulate beam attenuation to particle volume to estimate apparent density of sediment in suspension. Data from several studies are used to compare density estimates from the different methods. The new optical method produces apparent densities that are correlated linearly with measurements of the ratio of dry mass to wet volume. However, the new optical method produces density estimates that do not correlate with video estimates of apparent density. Lack of correlation is due to sampling bias of the video method, which has a relatively large lower limit of resolution in particle size. Development of a higher resolution camera would eliminate the current bias in particle size and would further validate the new optical method as an accurate proxy for apparent density.

List of Abbreviations and Symbols Used

Symbol	Parameter Definition and Units
c_p	Beam Attenuation (m^{-1})
c_p:*SPM ratio*	Beam Attenuation to SPM conversion ($m^2\ g^{-1}$)
D50	Median Particle Diameter (μm)
D	Elliptical Nominal Diameter (μm converted to m)
DFC	Digital Floc Camera
Dp	Component Particle Size (μm)
DVC	Digital Video Camera
DVC method	Established method for calculating apparent density of sediment in suspension. Requires size-settling velocity data from the DVC.
g	Gravitational acceleration ($m\ s^{-2}$)
LD method	LISST-DFC method for calculating apparent density of sediment in suspension. Requires only optics.
LISST	Sequoia Scientific LISST 100x laser particle sizer (Type B or Type C)
MINSSECT	Modified in Situ Size Settling Column Tripod
M_{Cp}	Mass converted from Beam Attenuation
M_s	Suspended Particulate Mass ($g\ m^{-3}$)
M_w	Mass of Seawater ($g\ m^{-3}$)
SPM	See M_s
SPM method	Established method for calculating apparent density of sediment in suspension. Requires collection of water.
V_f	Volume Fraction (Dimensionless)
V_s	Volume of Solids ($m^3\ m^{-3}$))
V_T	Total Merged Volume (Volume from the LISST and DFC ($m^3\ m^{-3}$))
V_{LISST}	Particle Volume Concentration (from the LISST only ($m^3\ m^{-3}$))
Ws	Settling Velocity ($mm\ s^{-1}$ converted to $m\ s^{-1}$)
WTS	Water Transfer System (McLane Research Laboratories, Inc. Phytoplankton Sampler)
δ	Component fractal dimension
μ	Viscosity ($kg\ (m\ s)^{-1}$)
ρ_a	Apparent Density ($kg\ m^{-3}$)
ρa_D	Apparent Density as a function of diameter ($kg\ m^{-3}$)
ρa_{DVC}	Apparent Density estimated from DVC method ($kg\ m^{-3}$)
ρa_{LD}	Apparent Density estimated from LD method ($kg\ m^{-3}$)
ρa_{Model}	Apparent Density estimated from the model approach ($kg\ m^{-3}$)

Symbol	Parameter Definition and Units
ρa_{SPM}	Apparent Density from observed measurements (kg m^{-3})
ρ_e	Effective Density (kg m^{-3})
ρ_f	Floc Density (kg m^{-3})
ρ_s	Component Particle Density (kg m^{-3})
ρ_w	Water Density (kg m^{-3})
γ	Rate that fractal dimension decreases with increasing particle size

Acknowledgements

The author would like to thank Dr. Paul Hill for the opportunity to work in the Hill lab and with this research. This project was made possible with the help of the following labs who contributed their time, effort, ideas and equipment: Hill lab and BIO Particle Dynamics Lab. The author would also like to thank the U.S. Office of Naval Research for providing funding for this project.

Chapter 1.0 - Introduction

1.1 Introduction

Small sediment particles in marine environments are often flocculated, which means that small particles adhere to one another, resulting in larger, composite particles, known as flocs [*McCave*, 1984; *Hill et al*., 2011]. Measuring floc properties is difficult because flocs are fragile and easily altered during sampling due to increased turbulence caused by sampling procedures [*Winterwerp and van Kesteren*, 2004]. Therefore, measurements must be carried out in situ and non-invasively in order to preserve natural particle size and apparent density.

Apparent density of particles in a suspension is the total dry mass of particles divided by the total wet volume of the particles. Apparent density affects average particle settling velocity, which is a fundamental variable for determining the deposition rate of sediment in suspension.

Two general methods have been applied to the estimation of apparent density. One method relies on collection and filtration of a known volume of water to estimate suspended particulate dry mass concentration (SPM) combined with particle sizing instruments to estimate particle volume [e.g., *Mikkelsen and Pejrup*., 2000]. The other method employs video imaging of settling particles to generate size versus settling velocity relationships that are used to reconstruct particle densities [e.g. *Hill et al*., 1998; *Sternberg et al*., 1999; *Mikkelsen and Pejrup* 2001; *Curran et al*., 2007].

With these methods it is difficult to construct high-resolution time series of apparent density. Estimation of particle dry mass via collection and filtration of water is laborious, imposing limits on the number of estimates of apparent density that can be generated. Video techniques involve the isolation of a water parcel for fixed periods, again limiting the temporal resolution of density estimates. Limited temporal resolution hampers the development of predictive models of apparent density.

The goal of this thesis is to explore a new method for estimating apparent density that uses in situ optical instruments. This method uses a Sequoia Scientific LISST 100x laser particle sizer (LISST) and a digital floc camera (DFC) to estimate particle volume concentration and measure particle beam attenuation (Figure 1.1). The particle beam attenuation is proportional to suspended particle mass concentration [*Snyder et al., 2008*; *Boss et al.*, 2009; *Neukermans et al.*, 2012]. With this knowledge, the assumption can be made that the ratio of beam attenuation to particle volume concentration is proportional to apparent density. Apparent densities obtained using the new method will be compared to those derived with the two established methods.

Figure 1.1: LISST and DFC profile package during the 2013 Hudson cruise to Minas Basin.

1.2 Background

Sediment transport, resuspension and deposition in aquatic environments are affected by several processes. Introduction of sediment into suspension can be accomplished by resuspension due to waves, resuspension due to tidal currents, resuspension due to lower frequency currents and influx of sediment-laden river discharge [e.g. *Ogston and Sternberg.*, 1999]. In coastal waters that are not proximal to rivers, waves and currents determine sediment resuspension and transport. A high correlation between wave orbital velocity and the concentration of sediment in a suspension characterizes resuspension due to waves. After sediment has been resuspended due to wave forcing, sediment is transported via currents [*Ogston and Sternberg.*, 1999]. Net sediment transport is often determined by low frequency (subtidal) currents (e.g. via storm events) rather than the higher frequency oscillations associated with tides and waves.

Due to the variety of mechanisms and associated frequencies driving sediment transport, long, high-resolution time series of sediment properties and forcing mechanisms are required to provide a better understanding of sediment dynamics. Particle settling velocity is affected significantly by apparent density, making apparent density a variable of interest as it determined clearance rate of a suspension.

One established method of estimating apparent density involves physical measurements of SPM as well as volume measurements from an instrument such as a LISST. Physical SPM measurements require filtration, drying and weighing in the

laboratory. Using the dried SPM samples and volume estimates from an optical instrument, apparent density (the ratio of dry weight to wet volume of particles) can be calculated [*Mikkelsen and Pejrup*., 2000; *Babin et al*., 2003]:

$$(\rho_f - \rho_w) \propto \frac{M_s}{V_t} \quad [1]$$

The left hand side of Equation 1 is the density of particles in excess of the density of water. This quantity is also referred to as the effective density (ρ_e, kg m^{-3}), where ρ_f is floc density and ρ_w is water density (both in kg m^{-3}). The right hand side of the equation is the apparent density *(ρ_a*, kg m^{-3}*)*, where M_s (also known as *SPM*) is the dry weight of sediment per unit of fluid volume (kg m^{-3}), and V_t is the total volume concentration of suspended particles (m^3 m^{-3}).

The effective density (ρ_e) is proportional to the apparent density (ρ_a) as shown in Equation 1. To understand how they are proportional, *Mikkelsen and Pejrup*. [2001] derived an expression for ρ_f:

$$\rho_f = \frac{M_w + M_s}{V_t} \quad [2]$$

where M_w is the mass of water within flocs (kg). Values for density terms in the following derivation are in units of kg m^{-3}, while units of volume are expressed in m^3. Assuming that flocs are composed of only water and the component solid particles, M_w

can be expanded to give the following:

$$M_w = \rho_w(V_t - V_s).$$

[3]

By substituting Equation 2 into Equation 3 we can solve for ρ_f:

$$\rho_f = \frac{\rho_w(V_t - V_s) + \rho_s V_s}{V_t} = \rho_w + (\rho_s - \rho_w)\left(\frac{V_s}{V_t}\right).$$

[4]

By subtracting ρ_w from each side of Equation 4 and by multiplying the resulting right hand side by (ρ_s/ρ_s), an alternate expression for effecting density results in the following:

$$\rho_e = \rho_f - \rho_w = \frac{(\rho_s - \rho_w)}{\rho_s}\left(\frac{\rho_s V_s}{V_t}\right).$$

[5]

With rearrangement of Equation 5 to solve for effective density, and with the relationship $M_s = \rho_s V_s$, the proportionality of effective density to apparent density can be calculated using the following:

$$\rho_e = \left(\frac{\rho_s - \rho_w}{\rho_s}\right)\rho_a.$$

[6]

$$\rho_a = \left(\frac{\rho_s}{\rho_s - \rho_w}\right)\rho_e.$$

[7]

In Equations 6 and 7 ρ_s is the particle component density, where a value of 2650 kg m^{-3} (density of quartz) is commonly used.

Another established method for estimating apparent density employs sequential imaging of particles in a settling column. Settling columns are partly or wholly isolated from the surrounding suspension while observations of size and settling velocity are collected [*Fennessy et al.*, 1994; *Fennessy et al.*, 1996; *Hill et al.*, 1998; *Mikkelsen et al.*, 2004; *Hill et al.*, 2011]. Particle size and settling velocity are used in a rearranged version of Stokes Law to solve for particle density. This method requires custom equipment that is not available to most laboratories and is invasive because it requires the suspension to enter an artificially calm environment. Currently, processing of data with this method is time consuming and not practical for the collection of large data sets due to lengthy data processing time.

A new proxy for apparent density makes use of measurements that can be made in situ and at high temporal resolution. This method uses two main instruments, a LISST and a Digital Floc Camera (DFC). The LISST measures beam attenuation (c_p, m^{-1}), which is proportional to SPM [*Snyder et al., 2008*; *Boss et al.*, 2009; *Downing*, 2006; *Hill et al.*, 2011; *Neukermans et al.*, 2012]. The beam attenuation is divided by the total merged volume (V_t) to generate a proxy for apparent density. The V_t is found by merging size

distributions from the LISST, which resolves smaller particles, with those from the DFC, which resolves larger particles.

1.3 Objectives

The main objective of this study is to assess whether the new optical proxy for apparent density is correlated with the particle densities estimated using the two established methods. The secondary objectives of this study are to present time series of the new proxy for apparent density and to explore the processes responsible for time variation of apparent density.

Chapter 2.0 - Methodology

2.1 Overview

In total, eight complete datasets from various sites around North America were analyzed. The term complete dataset includes data collected from the instruments required for the methods presented in this research. Data collection sites range in environment and included wave-stirred coastal environments, tidally dominated environments, and aquaculture sites (Table 2.1 and Figure 2.1).

The instrument platform for collection of the majority of the data sets is the Modified In Situ Size and Settling Column Tripod (MINSSECT). The MINSSECT is mounted with a Sequoia Scientific LISST 100x (Type B or Type C) laser particle sizer, a Digital Floc Camera (DFC), a Water Transfer System (WTS, McLane Research Laboratories, Inc. Phytoplankton Sampler) and a Digital Video Camera (DVC) for settling velocity measurements [*Hill et al.*, 2011]. Suspended particulate mass (SPM) is estimated from filters gathered with the WTS and sediment volume concentrations from the LISST and DFC. Equation 1 makes use the SPM measurements and the volume concentrations to estimate apparent density. This method for estimating apparent density is termed the SPM method. The DVC records video clips of sinking particles in the settling column. From these clips, size-settling velocity data are extracted and used to solve for apparent density. This method for estimating apparent density is termed the DVC method. The new optical method uses data only from the LISST and DFC. Beam attenuation is used as a proxy of mass, and using sediment volume concentration, apparent density can be

estimated using a similar equation to Equation 1. This method for estimating apparent density is termed the LD method. The comparison of the optical method to the established methods will be used to examine whether the LD method is a suitable proxy for apparent density (Figure 2.2). MINNSECT was deployed at each location for variable periods. With the exception of the Rivet 1 and Willapa experiments, all datasets were collected using MINNSECT. In Rivet 1, the DVC was deployed on a similar package to MINSSECT, while the LISST and DFC were mounted on a package that was profiled through the water column from a small boat. In Willapa Bay, data were collected the instruments mounted on smaller independent frames.

Experiment	Data Collection Location	Time of Data Collection	Environment Summary	Data Processing
Oasis 2007	Martha's Vineyard Coastal Observatory 12-m offshore node, Woods Hole, Massachusetts, US	Fall 2007	Wave-influenced nearshore bottom boundary layer	Archived
Willapa	Willapa Bay, Washington, US	Summer 2009	Mesotidal mud flat	Archived
Aqua 2010	Aquaculture Site, Bay of Fundy, New Brunswick, Canada	Summer 2010	Nearshore aquaculture site	Processed by Author
Oasis 2011	Martha's Vineyard Coastal Observatory 12-m offshore node, Woods Hole, Massachusetts, US	Fall 2011	Wave-influenced nearshore bottom boundary layer	DVC Data Processed by Author Merged Data Archived
Rivet 1	New River Inlet, North Carolina, US	Spring 2012	River inlet	Processed by Author
PARR 1	Aquaculture Site, Bay of Fundy, New Brunswick, Canada	Early Fall 2012	Nearshore aquaculture site	Processed by Author
PARR 2	Aquaculture Site, Bay of Fundy, New Brunswick, Canada	Late Fall 2012	Nearshore aquaculture site	Processed by Author
Hudson	Minas Basin, Canada	Summer 2013	Macrotidal estuary	Processed by Author

Table 2.1: Experiment summary outlining location and time of data collection in data collection. Data from Oasis 2007, Willapa, and merged data from Oasis 2011 were archived data. The remaining datasets were processed by the author.

2.2 DVC Method

A digital video camera (DVC) is used to measure settling velocity and particle diameter. The DVC is mounted to a settling column with a mechanized lid that closes at specified intervals. The height of the settling column is 51 cm, while the opening of the

column is 10x4cm. When the lid of the column is open, suspended sediment can enter, and the DVC does not record. When the lid closes, the camera begins to record video after 15 seconds. The lag in between closing time and start time allows flow-induced turbulence in the column to dissipate. In addition to the mechanized lid, the opening of the settling column is equipped with a baffled top (Figure 2.3). The mechanized lid and baffled top assist in minimizing the flow disruptions of settling particles within the column. The DVC records video on 80-min mini Digital Video (miniDV) tapes. During video capture, the DVC records 1-minute video clips.

The recovered miniDV tapes are processed in the laboratory. Video editing software (Sony Imageshaker) is used to separate and create digital copies of each recorded clip [*Mikkelsen et al*., 2004]. The 1-minute digital clips are loaded one at a time and examined for the presence of settling particles or any irregularities, such as upward or oscillating particle trajectories, which indicate inadequate isolation of the settling column from the surrounding environment. After observation, the user chooses a 4-second section in the video that is identified as representative of the particles in the entire video. From the 4-second section, four frames are captured, with a 1-second spacing. A final frame is captured at the end of the clip for the purpose of subtracting any stationary objects in the windows of the DVC. The five images are converted to binary images, using a greyscale threshold to identify particle edges [*Fox et al*., 2004; *Mikkelsen et al*., 2004]. Otsu's method [*Otsu*, 1979] is used to generate the initial threshold values for a set of images, but the threshold can be adjusted by the user if the particle outlines in the binary images are not similar in shape or size to the original

images. Particles in each image are numbered and tagged sequentially. Particle tags are placed into the image, with a different colour for each image. The four tagged images are combined, and tracks are recorded by entering the colour-coded numbers in a txt file. A particle's first appearance is tagged with a red number, while the second, third and fourth appearances are tagged with green, blue and yellow numbers respectively (Figure 2.4). A minimum of three particle appearances in a particle track is required for analysis. The text file containing the particle tags for each track is used to extract nominal diameter, settling time, settling distance and settling velocity [*Fox et al*., 2004; *Hill et al*., 2011].

Stokes Law is used to estimate effective density for each particle (Equation 8):

$$(\rho_f - \rho_w) = \left(\frac{Ws * 18\mu}{g * D^2}\right) \quad [8]$$

The variable W_s is the settling velocity (m/s), μ is the dynamic viscosity (kg (m s)$^{-1}$), g is acceleration due to gravity (9.8 m s^{-2}), and D is the equivalent circular diameter of the particle (m). The dynamic viscosity was calculated using a global temperature and salinity of 10 °C and 25 ppt respectively. The left hand side of the equation is equal to ρ_e. If Equation 8 is substituted into Equation 7, then apparent density can be calculated using the following:

$$\rho_a = \left(\frac{Ws * 18\mu}{g * D^2}\right)\left(\frac{\rho_s}{\rho_s - \rho_w}\right).$$

[9]

For this equation, a value of 2650 kg m^{-3} (density of quartz) is used for ρ_s. The assumption that the apparent densities in Equations 1 and 9 are equal will be true if the sizes of sediment in suspension lie within the resolution limits of the DVC, where the minimum resolvable particle diameter is 180 µm [Mikkelsen et al., 2004].

Figure 2.1: Locator map of data collection sites across North America. The data collection sites are: MVCO 12-m node (1), New River Inlet (2), Minas Basin (3), the Bay of Fundy (4), and Willapa Bay (5).

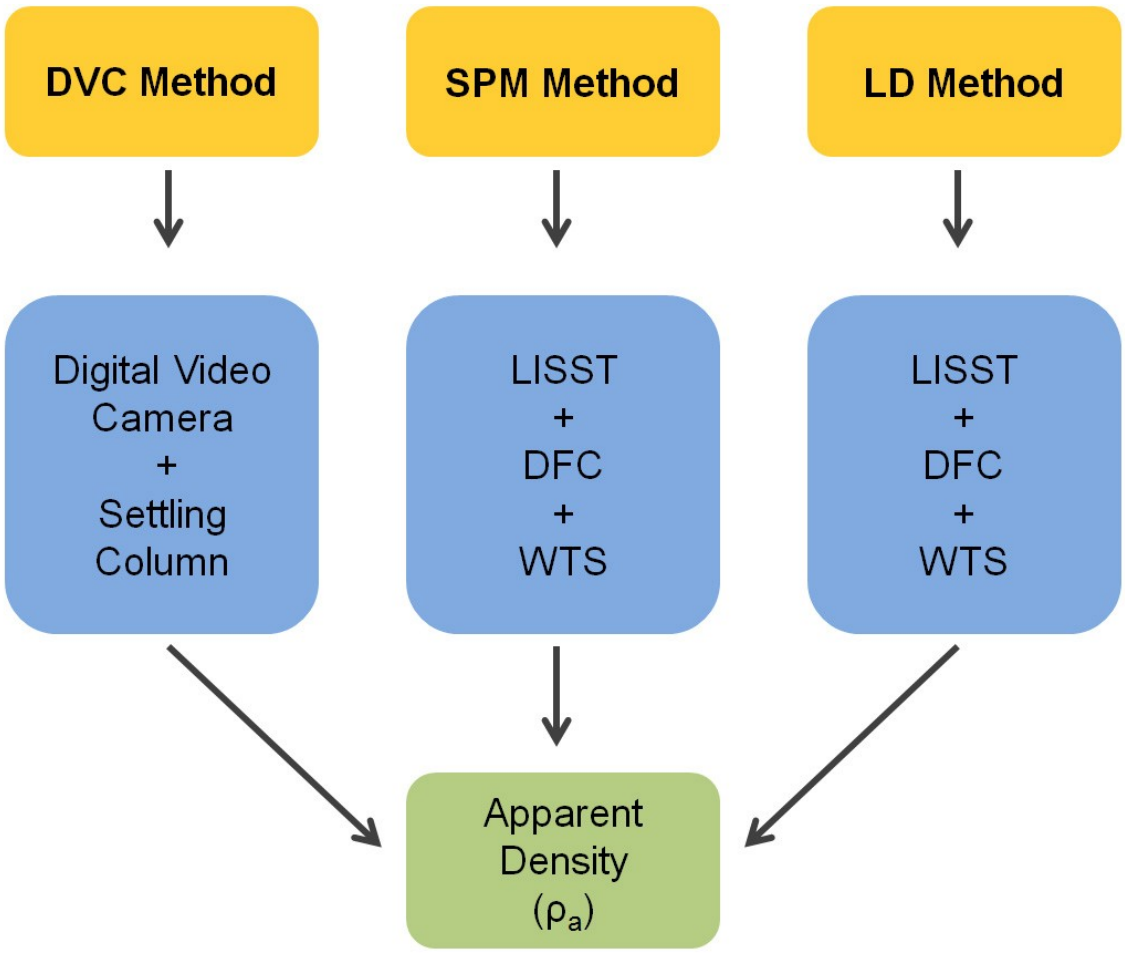

Figure 2.2: Flowchart illustrating the methods used in this research, including the instruments and variable of interest. The DVC Method uses a Digital Video Camera (DVC) that is equipped with a settling column. The SPM Method uses a combination of instruments that include a LISST, a Digital Floc Camera (DFC), and a Water Transfer System (WTS). The LD method uses the same instrument combination as the SPM method but uses beam attenuation as a proxy for dried sediment mass.

Figure 2.3: Top of the settling column of the DVC. The baffle on the top of the column (honeycomb structure) minimizes flow disturbance when the column is open. Prior to collection of video data, a mechanized lid is moved into position over the column. The lid limits the effect of turbulent stirring or wave pumping on the downward trajectories of particles in the column.

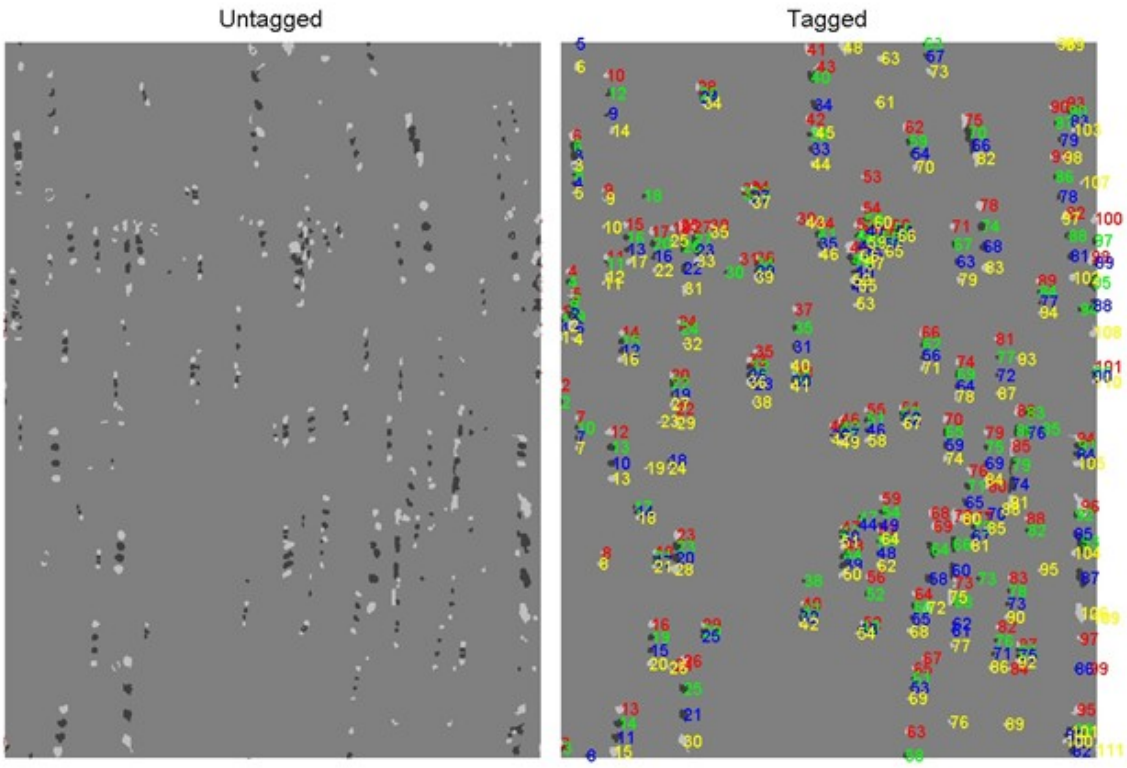

Figure 2.4: Composite images from Oasis 2011, deployment 2, clip 34: Left) Untagged composite image comprising four frames each separated by 1 second; Right) Tagged composite images where the colour of a number-tagged particle depends on the frame in which it was found. Red tags indicate frame 1. Green, blue and yellow tags indicates frames 2, 3 and 4 respectively. Particle tracks are constructed from the image with tagged particles. The numbers of the coloured tags are recorded and are used to determine settling velocity and particle size.

2.3 LD Method

The proposed optical proxy for apparent density is referred to as the LD method, because it uses a **L**ISST and **D**FC combination to estimate particle dry mass and wet volume concentrations. Together, these instruments resolve a particle diameter range of 1.25 µm to 4 cm for LISST B and 2.50 µm to 4 cm for LISST C [*Hill et al*., 2011]. The LISST, an instrument from Sequoia Scientific, estimates beam attenuation (c_p, m^{-1}) and particle volume concentrations over particle diameters ranging from 1.25 to 250 µm for type B and 2.5 to 500 µm for type C [*Mikkelsen et al*., 2005; *Hill et al*., 2011; *Neukermans et al*., 2012]. Software from Sequoia Scientific is used to invert the scattered light measurements to determine particle size distribution and to calculate the beam attenuation coefficient. The software provided from Sequoia uses a spherical scattering property kernel matrix. To calculate the beam attenuation coefficient, the software calculates the ratio of the transmitted light intensity to the transmitted light intensity in particle-free water [*Mikkelsen et al*., 2005; *Hill et al*., 2011]. This method accounts for attenuation due to water. The light transmitted by the LISST has a wavelength of 670 µm, which reduces light attenuation from dissolved substances. Assuming that attenuation due to water and attenuation due to dissolved substances have been addressed, the beam attenuation coefficient can be used as an estimate of the particulate beam attenuation coefficient.

The DFC measures particles with diameters that range from 45 µm to 4 cm. It captures images of suspended particles with silhouette photography at identical time

intervals as the LISST. These images are captured as water flows through a 4 x 4 x 2.5 cm gap between two glass plates [*Mikkelsen et al*., 2004; *Mikkelsen et al*., 2005; *Hill et al*., 2011]. After recovery, images are examined for quality, and photos that are not satisfactory are removed. Images that are removed during quality control are those that contain bubbles, long organics, large organics (e.g. fish), and digitally corrupted, incomplete images. After this quality assessment, an area of interest (AOI) is chosen for a single deployment or series of deployments. The AOI is chosen to reduce the amount of stationary debris in the images [*Hill et al*., 2011]. Software written in Matlab takes the acceptable colour images, crops them and converts them to grey scale. Variation in background pixel intensity is reduced by applying a top-hat filter to the images. Particles are distinguished from the background using Otsu's method [*Otsu*, 1979; *Hill et al*., 2011]. Particle areas are calculated and converted to equivalent spherical volumes and diameters. Stationary debris can be subtracted over a series of images. Average pixel intensities in 6-hour bins are calculated, and pixels that are consistently darker than other pixels are identified as stationary debris on the camera windows and removed from the analysis.

Merging the LISST and DFC data is accomplished by first distributing the equivalent spherical volumes into 57 bins based on diameter, using another Matlab script. Specified lower size bins of the DFC are joined with specified upper size bins of the LISST via linear interpolation (Table 2.2) in log space, producing a merged size distribution that covers particle diameters from 1.25 µm to over 4 cm for LISST B or 2.50 µm to over 4 cm for LISST C.

Experiment	Interpolation Bin Range
Oasis 2007	23:32
Willapa	Unknown
Aqua 2010	16:22
Oasis 2011	16:22
Rivet 1	16:22
PARR 1	Type B: 21:27 Type C: 16:22
PARR 2	21:27
Hudson	23:27

Table 2.2: Summary of the range over which linear interpolation occurs. The left column contains the experiment while the right column contains the range of bins that were interpolated. Range of linear interpolation for merged distributions varies because of different models of the DFC and LISST used in the various experiments. The bin range for the Willapa is unknown because it is an archived data set and the information on bin range is not available.

The LD method assumes that beam attenuation is proportional to mass in suspension [*Boss et al.*, 2009; *Hill et al*., 2011]. Therefore, an empirical conversion is used to approximate mass. This is done by plotting c_p (m^{-1}) versus *SPM* (see M_s) and applying a linear regression. The slope of the regression equals the c_p*:SPM* ratio. For the purposes of this research, a c_p*:SPM* ratio of 1 is used, which simply assumes that the two quantities are proportional. In other words, the apparent density estimated using the LD method is the ratio of c_p*:*V_t. Therefore, Equation 10 is used to solve for mass (M_{Cp}) using beam attenuation, where c_p*:SPM* is equal to 1:

$$M_{Cp} = \frac{c_p}{c_p{:}\,SPM}\,. \qquad [10]$$

Using the mass calculated in Equation 10, the right side of Equation 1 can be modified by replacing M_s with M_{Cp} from Equation 10 to solve for apparent density, which is calculated as c_p:V_t in this research:

$$\rho_a = \frac{M_{C_p}}{V_t} \propto \frac{c_p}{V_t} \quad [11]$$

The data collected from the LISST and DFC has been summarized in Table 2.3. There were two main mechanisms of deployment for the LISST and DFC packages. The first method of deployment was a stationary deployment, where the LISST, DFC and DVC were all deployed on the same package and left for a period of time to collect data. The second deployment mechanism was a cast deployment and involved a smaller package with only the LISST and DFC. In this deployment method, the DVC was deployed and was stationary for a given time period while the LISST/DFC package was profiled repeatedly in the vicinity of the DVC.

Experiment	Deployment Type	LISST Type	Number of Merged Size Distributions
Oasis 2007	Stationary	Type B	5725
Willapa	Stationary	Type B	1399
Aqua 2010	Stationary	Type C	7145
Oasis 2011	Stationary	Type C	3814
Rivet 1	Cast	Type C	1176
PARR 1	Stationary	Type B (Deployment 2) and Type C (Deployment 1 and 3)	Type B: 1074 Type C: 2859
PARR 2	Stationary	Type B	4339
Hudson	Stationary	Type B	1799

Table 2.3: Summary table of data collected from instruments used in the LD method. Summary includes: the deployment type, the LISST type that was used, and the total number of merged size distributions.

2.4 Suspended Particulate Mass Collection

This study uses two primary methods to obtain a direct estimate of suspended particulate mass (SPM, mg L^{-1}) concentration. It should be noted that M_s and *SPM* are the same quantity. The first method uses a McLane Research Laboratories Inc. Phytoplankton Sampler water transfer system (WTS) to directly estimate SPM. The SPM is obtained from 24 filter samples held by the WTS. At regular intervals, a specified volume of sediment-laden water is passed through a filter. The filters used are pre-weighed Millipore 8.0 µm SCWP (cellulose acetate). These were selected on the basis of small operational pore sizes and reduced clogging [*Hill et al.*, 2011]. Prior to deployment, the WTS is flushed with water to clean the tubes of any debris. The air in the WTS is then flushed out using super Q water, resulting in a sealed system. The second method for measuring SPM involves the collection water samples using Niskin

bottles. The SPM samples retrieved from Niskin bottles are collected at the same depth and location of the instrument package containing the LISST, DFC and DVC.

2.5 Model Approach

To address the possibility that the DVC method estimates of apparent density are biased to larger particle sizes, a third approach was taken to estimate apparent density that combined the data collected from the DVC, the LISST and the DFC. This approach fit a model to the data collected from the DVC and extrapolated the model fit to estimate apparent density across the full range of particle diameters [*Hill et al.*, 2011]. Specifically, there are two models of particle geometry and fluid drag that can be fit to the DVC data [*Khelifa and Hill*, 2006; *Maggi*, 2013]. This study uses a simplified version of the model presented by *Maggi* [2013] because it does not require the components of flocs to be solid particles.

To describe the settling velocity of particles in suspension, a simple force balance can be used to determine the variables that determine particle settling velocity [*Khelifa and Hill*, 2006; *Maggi*, 2013]. This is a force balance between gravitational (F_g), buoyancy (F_b) and drag forces (F_d):

$$F_g - F_b = F_d \ . \qquad [12]$$

Equation 12 can be further expanded by separating the components that compose the drag force, which are inertial forces (F_i) and viscous forces (F_v) [*Rubey 1933*; *Maggi 2013*]:

$$F_g - F_b = F_v + F_i \ .$$

[13]

In this equation, the viscous force corresponds to the force required to shear the fluid near the particle surface. The inertial force describes the force required to displace the volume of the fluid through which a particle is passing [*Maggi 2013*]. For spheres, the following equations from *Maggi* [2013] represent how the force balance can be expanded:

$$F_g = \frac{4}{3}\pi(\frac{D}{2})^3\rho_s g;$$

[14]

$$F_b = \frac{4}{3}\pi(\frac{D}{2})^3\rho_w g;$$

[15]

$$F_v = 6\pi(\frac{D}{2})\mu W_{s;}$$

[16]

$$F_i = \pi(\frac{D}{2})^2 \rho_w {W_s}^2 .$$

[17]

In equations 14-17, W_s is the settling velocity, D is the particle diameter, μ is the dynamic viscosity of the fluid, g is the gravitational constant, ρ_s is the component particle density, and ρ_w is the density of the fluid. When solving for W_s, the quadratic formula is used and results in the following equation:

$$W_s = \frac{-18\mu + \sqrt{(18 * \mu)^2 + 6 * g * D^3 * \rho_w(\rho_s - \rho_w)}}{3 * D * \rho_w}.$$

[18]

Equation 18 was presented by *Rubey* [1933], for single solid particles. Because many sediment particles in suspension are actually particle aggregates (flocs), Equation 18 needs to be modified to address the internal geometry of flocs [*Khelifa and Hill*, 2006; *Maggi*, 2013]. This expansion has been derived in detail by *Maggi* [2013], and assuming spherical geometry, results in the following equation:

$$W_s = \frac{-18\mu + \sqrt{(18 * \mu)^2 + \left(6 * g * {D_p}^3 * \rho_w(\rho_s - \rho_w)\right) * l^{D_f}}}{3 * D * \rho_w}.$$

[19]

In Equation 19, D_p is the size of the primary particles that comprise flocs, l is the dimensionless aggregate size (D/D_p), and D_f is the fractal dimension, which is defined by the following [*Maggi*, 2013]:

$$D_f = \delta * l^{\gamma}. \qquad [20]$$

In Equation 20, δ corresponds to the component particle fractal dimension and γ corresponds to the rate at which the fractal dimension decreases with increasing particle size.

Equation 19 is fit to size-settling velocity data gathered with the DVC with the function lsqcurvefit in Matlab 2009b. The variables that are estimated are ρ_s, D_p, δ and γ. Initial estimates must be provided to initialize the fitting function. In this study, two sets of input parameters were used, an upper bounds (UB), where dense solid particles are assumed, and a lower bounds (LB), where less dense organics are assumed. The values used for the upper and lower bounds are outlined in Table 2.4. The upper and lower bounds are also used as the constraint limits for the curve to fit. Therefore, one model run would use the upper bounds as the initial parameters, while using the upper and lower bounds as values to constrain the parameter values. The second run of the model uses the lower bounds as initial parameters, while using the upper and lower bounds as values to constrain the parameter values. The viscosity of sea water (μ), was calculated using a uniform temperature and salinity in Matlab.

The goal is to generate a general fit that can be applied to all datasets. To accomplish this, data from all studies were combined to obtain best-fit estimates of ρ_s, Dp, δ and γ.

Limits	$\boldsymbol{\rho_s}$ *(Component Particle Density)*	***Dp*** *(Component Particle Size)*	$\boldsymbol{\delta}$ *(Component fractal dimension)*	$\boldsymbol{\gamma}$ *(Rate that fractal dimension decreases with increasing particle size)*
Upper Bounds	2650 (kg m^{-3})	1.0E-05 (m)	3 (dimensionless)	0 (dimensionless)
Lower Bounds	1100 (kg m^{-3})	2.0E-06 (m)	1 (dimensionless)	-0.1 (dimensionless)

Table 2.4: Initial input parameters for the settling velocity model. the parameter ρ_s is the component particle density, Dp is the component particle size, δ is the component particle fractal dimension and γ is the rate that the fractal dimension decreases with increasing particle size.

A second model is used to calculate apparent density. The model uses the best-fit settling velocity coefficients (ρ_s, Dp, δ and γ):

$$\rho a_D = \rho_s * l^{D_f - 3}. \quad [21]$$

In the above equation, ρa_D represents the apparent density as a function of diameter. This is used with combination of the size distributions from the LISST and DFC to estimate apparent density for the entire size distribution by summation of the product of volume fraction and the ρa_D in Equation 21 to solve for ρ_a.

2.6 Data Correction

During data collection and processing, corrections were necessary for some of the data sets. The datasets that needed to be corrected were those from the following experiments: Oasis 2011, Aqua 2010 and Hudson. During the deployments of Oasis 2011, barnacle growth was observed on the instruments of MINSSECT. This growth affected the c_p and volume concentration data collected by the LISST and DFC. Barnacle growth produced artificially high c_p's and volume concentrations, which increased exponentially during the deployment. To correct for this with the LISST data, an exponential fit was applied to the attenuation data, and then subtracted from the data. For the DFC data, the effect of barnacles was removed via the background subtraction process outlined previously in section 2.3. This background subtraction can lower volume concentrations, as the barnacles mask the presence of any particles in the portions of the images covered by barnacles. It should be noted that for the LISST volume concentration data, only bins 27 to 32 of the 32 LISST size bins were affected by barnacle fouling, and these bins are not used in the merged particle size distributions.

During the deployments of the Aqua 2010 experiment, biofouling was observed on the DFC. The fouling observed on the DFC was mostly composed of organisms which were not completely stationary, so background subtraction was not effective. Therefore, the merged data from Aqua 2010 were dropped from analysis. However, the DVC data from Aqua 2010 were useable, so they were included in the development of a fractal settling model.

During the Hudson experiment, negative c_p values were observed. Although the LISST is calibrated for clear water (section 2.3), the c_p's recorded by the LISST during this experiment were lower than that of the calibration. To correct for this, a new clear water transmission value was calculated. The new clear water value of transmission was then used to recalculate beam attenuation coefficients.

Chapter 3.0 - Results

3.1 Overview

In this study, data were collected in a variety of depositional environments, with a range of weather forcing. This variety resulted in variable particles sizes, size-settling velocities and water conditions. The range in conditions allows for a reasonable assessment of the validity of the LD method as a replacement for the established methods (DVC method and SPM method). Comparison of the LD method against the established methods yields conflicting results. Results from the model approach offer explanation for the differences between the LD and DVC method and are similar to the results of the SPM method.

3.2 DVC Method

A summary of the data collected from the DVC is in Table 3.1, while the archived data can be found accompanying this file on DalSpace. The number of particles tracked in a given experiment is affected by the presence of particles (i.e. lower sediment concentration means fewer particles tracked), number of deployments, and recoverable data. A total of 22335 particles were tracked in this research across different depositional environments, and similarities can be observed among the individual experiments. Median settling velocities ranged from 0.58 mm s^{-1} to 1.13 mm s^{-1}, while median particle diameters range from 300 µm to 400 µm. Median apparent densities range from 15 kg m^{-3} to 45 kg m^{-3}.

Experiment	Video Clips	Particles Tracked	Median Settling Velocity (mm s^{-1})	Median Particle Diameter (μm)	Median Apparent Density (kg m^{-3})
Oasis 2007	315	7606	1.06	400	27
Willapa	93	3398	1.13	320	40
Aqua 2010	58	412	0.58	340	15
Oasis 2011	104	2242	0.82	370	26
Rivet 1	52	777	0.88	310	43
PARR 1	195	3748	0.81	320	29
PARR 2	114	2565	0.89	300	33
Hudson	73	1587	1.10	310	45

Table 3.1: Summary table of DVC data. Experiments are in chronological order.

3.3 SPM Method

Individual values of SPM and apparent densities estimated using this method are contained in the accompanying file on DalSpace. A summary of the data collected using this method is contained in Table 3.2. In total, 377 SPM samples were collected across all of the included experiments in Table 3.2. Median SPM values range from 2.67 mg L^{-1} to 6.25 mg L^{-1}, while median densities ranged from 24 kg m^{-3} to 360 kg m^{-3}. Unlike the relatively small range and values of the median apparent densities from the DVC method, the range and median values using the SPM method are significantly greater. This observation indicates that the DVC is biased to larger particle aggregates, which decrease in density with increasing particle size [*Hill et al*., 1998; *Agrawal and Pottsmith*, 2000]. This result is addressed by the model approach, as it fits the DVC data to the entire size distribution.

Experiment	Number of SPM Data Points	Median SPM ($mg\ L^{-1}$)	Median Apparent Density ($kg\ m^{-3}$)
Oasis 2007	121	2.74	240
Oasis 2011	114	5.60	24
PARR 1	48	6.25	Type B: 240 Type C: 360
PARR 2	70	3.97	190
Hudson	24	2.67	240

Table 3.2: Summary table of estimates of apparent density based on measured SPM.

3.4 LD Method

Individual values collected from the LISST and DFC are contained in the accompanying file on DalSpace. The merged data (from the LISST and DFC) are summarized in Table 3.3. The total number of merged data points that were collected throughout all experiments was 29330. The median diameters (D50) range from 150 µm to 300 µm and the median apparent densities range from 15 kg m^{-3} to 100 kg m^{-3}. When comparing the summarized results to those of the established method, significant differences can be observed. When comparing the median apparent densities from Table 3.3 to those of Table 3.1 (DVC method), the DVC, on average, images less dense particles than the LD method. The DVC also records larger particle aggregates.

Experiment	Number of Merged Data Points	Median D50 (μm)	Median Apparent Density (kg m^{-3})
Willapa	1399	140	65
Oasis 2007	5725	270	100
Oasis 2011	3814	270	15
Rivet 1	1176	160	44
PARR 1	Type B: 1074 Type C: 2859	Type B: 140 Type C: 140	Type B: 32 Type C: 91
PARR 2	4339	290	70
Hudson	1799	300	29

Table 3.3: Summary table of merged data used in the LD method.

3.5 Established Methods Versus LD Method

The comparison between the DVC method and the LD method is done based on sampling time. After the particle tracks are processed, the apparent densities are calculated for all data points. The median of apparent densities is taken for each clip, creating one density for a given sample time. The apparent densities from the LD method are calculated for all merged data size distributions within ± 5 minutes of the DVC sampling time.

The Shapiro-Wilk test rejects the hypothesis that the apparent densities estimated using all three methods are normally or lognormally distributed ($p < 0.05$). Due to this result, when calculating the correlation coefficient, the nonparametric Spearman's rho was used.

Apparent densities estimates by the DVC method and the LD method are not correlated ($p = 0.28$) (Table 3.4 and Figure 3.1). Density estimates from the LD and SPM methods are correlated ($p = 0$) (Table 3.4). Logarithmic transformation was used to linearize the data while equalizing the variance. A Type II regression was applied to the

transformed data. The slope of the regression line is 1.05, with 95% confidence intervals of 0.95 and 1.16. These results indicate that the relationship between the LD method and the SPM method is not significantly different from a linear relationship (Figure 3.2).

Method Comparison	Number of data points	Correlation Coefficient (r)	p Value
LD vs DVC	1116	-0.04	0.28
LD vs SPM	425	0.51	0
Model vs SPM	425	0.61	0

Table 3.4: Data table of the results from the correlation analysis using Spearman's rho for the LD method versus the DVC method and the LD method versus the SPM method.

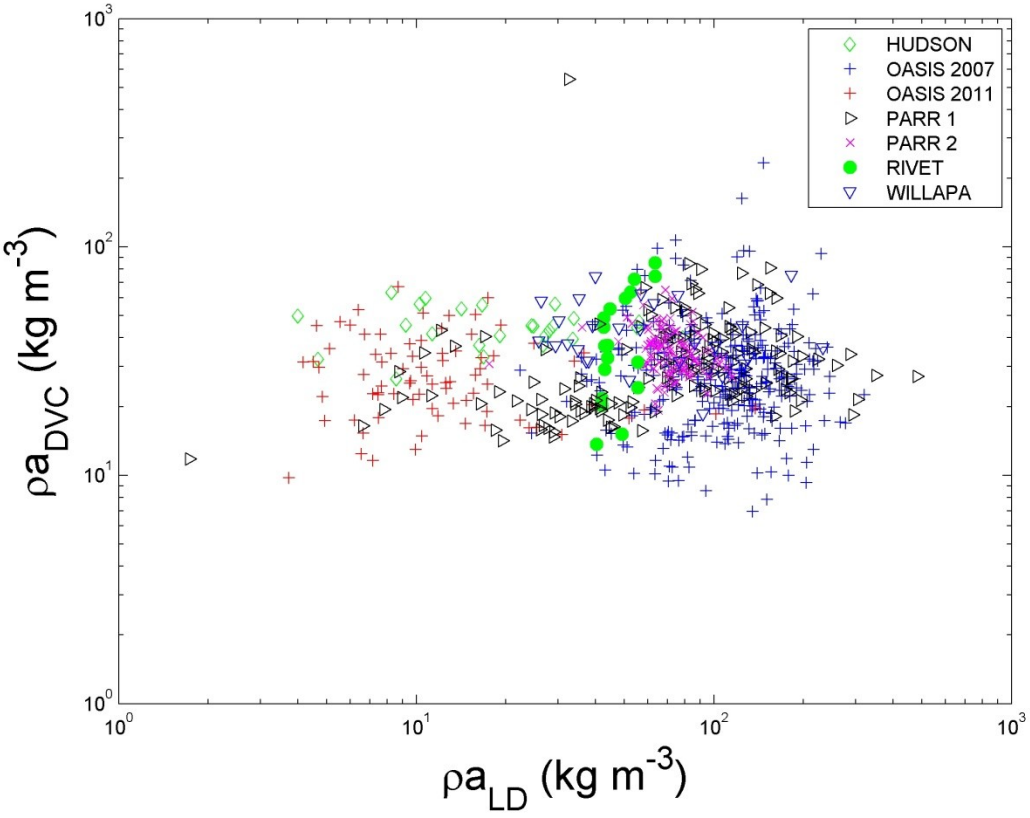

Figure 3.1: Apparent density estimated with the DVC method and the LD method on logarithmic scales. The p value of 0.28 is significantly greater than 0.05, which indicates that there is not a correlation between the two methods.

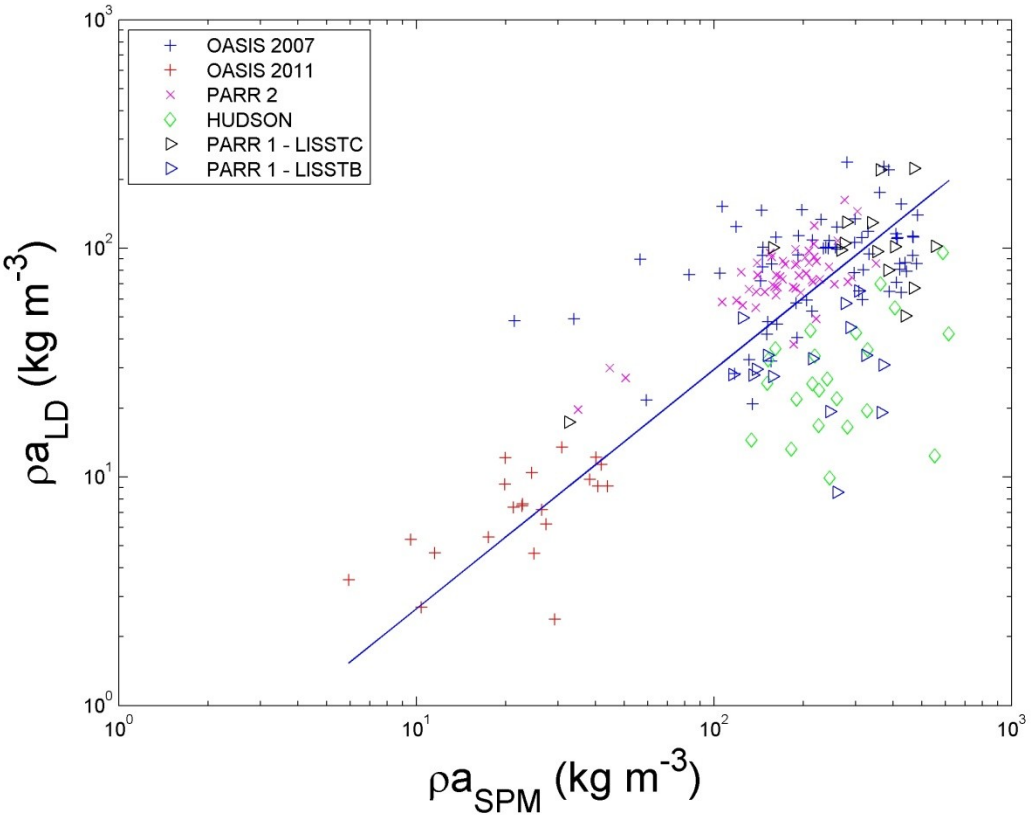

Figure 3.2: Apparent density estimated with the SPM method and the LD method in logarithmic scale. The slope of the Type II regression was equal to 1.05, with 95% confidence intervals of 0.95 and 1.16, which implied that these two estimates of apparent density are not significantly different from a linear relationship.

3.6 Model Approach

The fit that used the upper limit input parameters was similar to that of the lower limit input parameters. The complete results from the fractal settling model for the both the generalized upper limit and lower limit input parameters are contained in Table 3.5. As Figure 3.3 and Table 3.5 illustrate, the fits were almost identical. Both of the fits indicate that component particle density was similar to inorganic solid particle densities, and fractal dimensions were approximately 2 and did not vary with size. The upper limit input parameters were used to estimate particle density as a function of particle diameter.

Fractal Settling Model Results				
Experiment	ρ_s *(Component Particle Density)*	***Dp*** *(Component Particle Size)*	δ *(Component fractal dimension)*	γ *(Rate that fractal dimension decreases with increasing particle size)*
Upper Limit	2600 (kg m^{-3})	9.80E-06 (m)	1.80 (dimensionless)	-4.10E-14 (dimensionless)
Lower Limit	2600 (kg m^{-3})	9.90E-06 (m)	1.80 (dimensionless)	-4.00E-14 (dimensionless)

Table 3.5: Data table of the results from the Fractal Settling model using all datasets as one complete dataset. This table includes the results of the Fractal Settling velocity model using the upper limit and lower limit input parameters.

The parameters in Table 3.5 were used as input parameters in the fractal density model to generate apparent density (Equation 21). The volume used in this estimate is the total merged volume from the LD method. The median of volumes is taken within ±1 minute of SPM sample times. This tolerance was chosen to optimize accuracy of volume estimates, therefore increasing the accuracy of SPM method apparent density

estimates. It should be noted that results from experiments Rivet, Willapa and Aquaculture 2010 have been omitted in the comparison of model density to observed density. In Rivet, the results are omitted from this comparison for two reasons. The first is that the SPM samples were not collected using the WTS system but rather using Niskin bottles. The second is due to the deployment method of the instruments using the LD method. The instruments were deployed during a series of casts, rather than left at a stationary depth with the DVC for an entire deployment. Results from the Willapa experiment are also omitted, which is simply due to the absence of SPM measurements. Finally, Aquaculture 2010 was omitted due to biofouling on the DFC and LISST.

Density estimates from the model and SPM methods are correlated ($p = 0$) (Table 3.4 and Figure 3.4). However, the correlation between the two methods is not linear. Instead they are related via an exponential expression with an exponent that is less than 1.

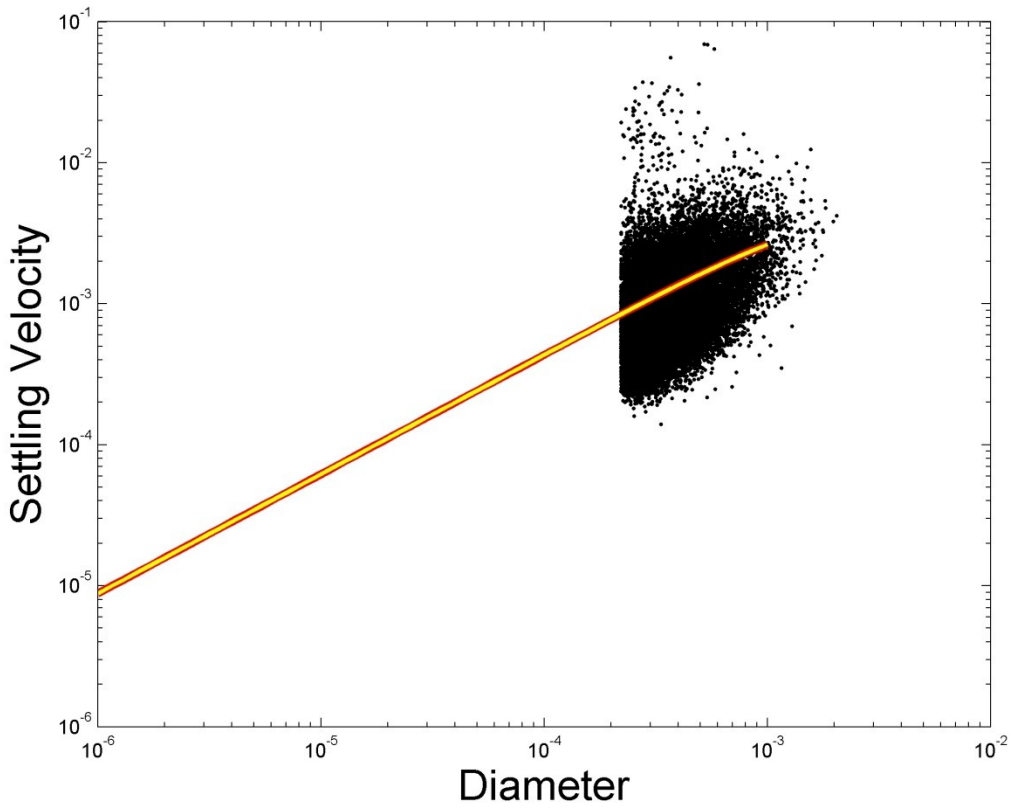

Figure 3.3: Results from the Fractal Settling model when treating all of the data as one dataset. The x-axis and y-axis represents diameter (m) and settling velocity (m s^{-1}) measured using the DVC. The thick red line represents the fit given by using the upper limit as the starting parameters, while the thin yellow line represents the fit given by using the lower limit as the starting parameters. This figure illustrates that using either limit as the initial parameters provides similar results to be used in the Density model. Therefore, for simplicity, the upper limit coefficients are used in the Fractal Density model.

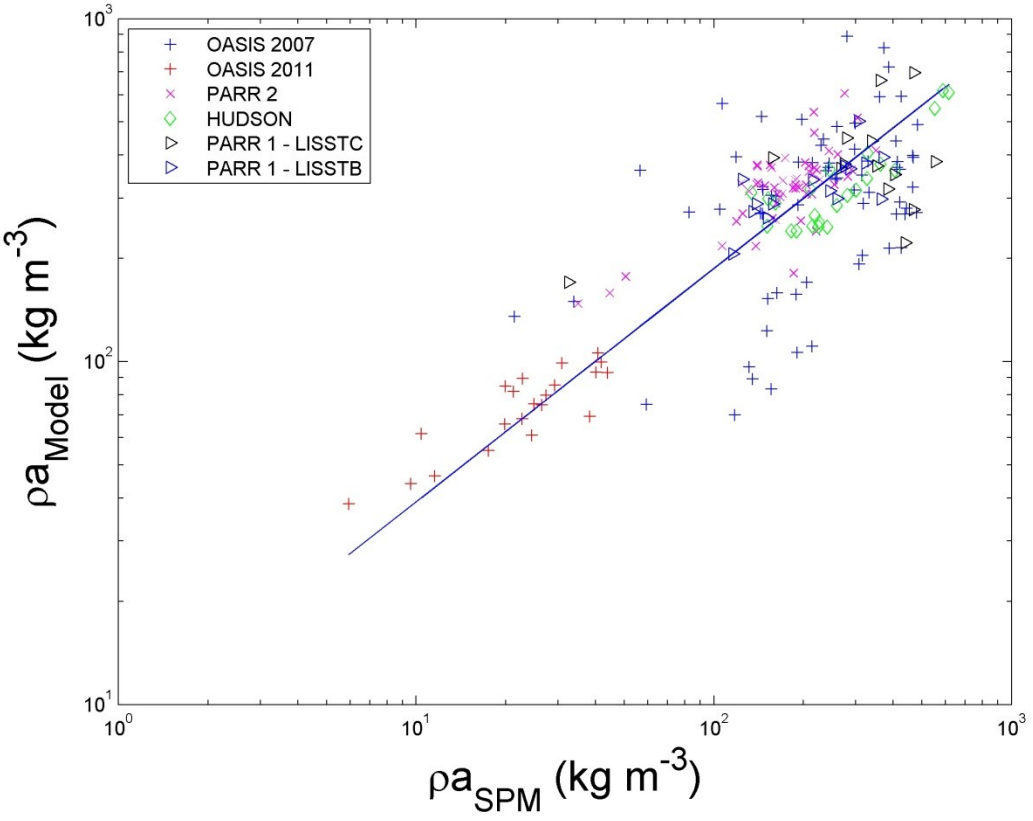

Figure 3.4: Modeled apparent density results compared with SPM method apparent density results on logarithmic scale. The slope is equal 0.68, with 95% confidence intervals of 0.62 and 0.74, which indicates that there is a nonlinear, exponential relationship between the apparent densities estimated using the Model method and the apparent densities estimated using the SPM method.

Chapter 4.0 - Discussion

4.1 DVC Method Versus LD Method

The comparison of apparent densities estimated using the DVC method versus the apparent densities estimated from the LD method yields results that do not correlate. Lack of correlation between the density estimates likely arises because the DVC, with a lower limit of resolution approximately equal to 180 µm, is biased toward large, lower density flocs. This hypothesis can be addressed by examining apparent densities from each method as functions of the median diameter (D50) at the same sampling time (Figure 4.1). Median diameters were derived from volume concentration estimates from the LD method. Apparent density estimated using the LD method increases with decreasing particle diameter (Figure 4.1), which is due to the fact that particles in suspension are aggregates. As the particle aggregates grow in diameter, the apparent density decreases [*McCave*, 1984]. For densities estimated with the DVC, however, no correlation exists between apparent density and median diameter (Figure 4.1). Lack of correlation indicates that the DVC observes particles with similar apparent density, because the DVC is unable to observe particles smaller than 180 µm. As a result, the DVC estimates remain relatively constant over a range of median diameters. Large aggregates have apparent densities that are similar.

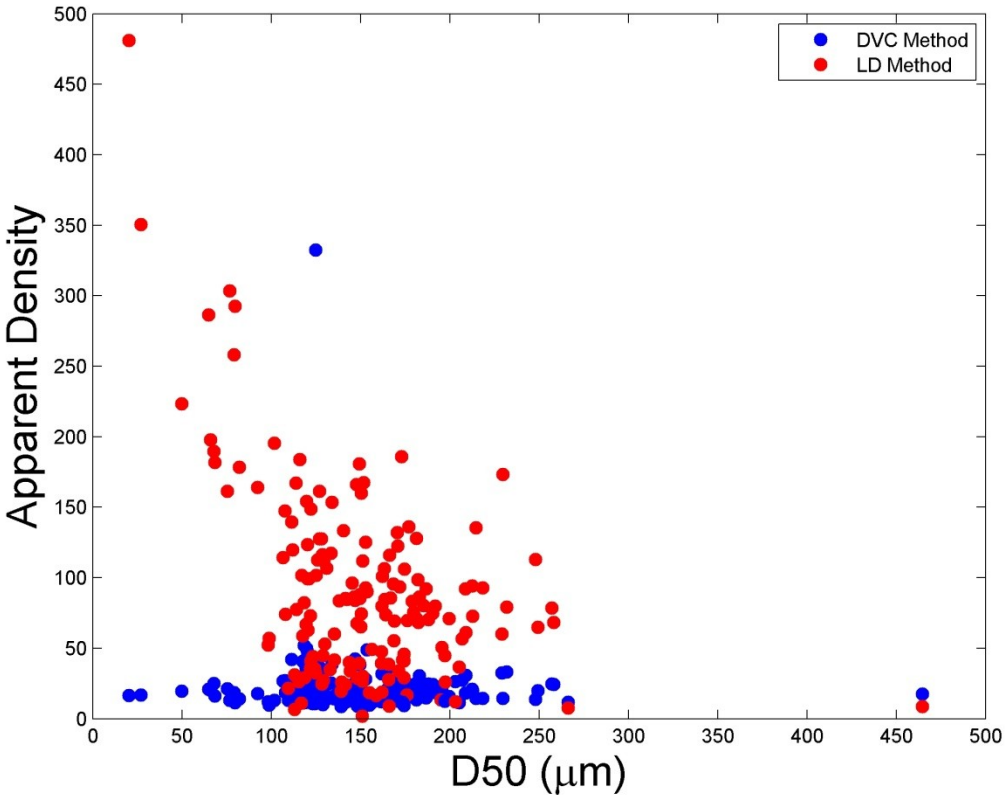

Figure 4.1: Median diameter (D50) from LD method volume concentrations against apparent density estimates from both the DVC method and the LD method. As the median diameter decreases in the LD method, there is a resulting increase in apparent density. Conversely, the apparent densities for the DVC method are relatively constant, regardless of the median diameter from the volume concentrations.

4.2 LD Method Versus SPM Method

The comparison of apparent densities estimated using the LD method versus the apparent densities estimated from the SPM method yielded a linear correlation. This is significant because it validates the LD method as a reasonable proxy for apparent density. Even more promising is that the apparent densities estimated using the LD method use a c_p:*SPM* ratio of 1. This means that c_p:V_t can be used as an accurate proxy for apparent density without the collection of SPM. However, correlation between the LD method and DVC method would further validate the LD method as an accurate apparent density proxy because the SPM method uses the particle volume concentrations that are used in the LD method. The measurements used in the DVC method are independent of those used in the LD method, therefore correlation between these two methods is required to determine if the LD method is a suitable addition to the established methods.

4.3 Model Results

Modeled apparent densities are derived by extending the estimates of density from the DVC to smaller size classes. The model densities correlate with the SPM method densities, providing more support for the hypothesis that the bias of the DVC to larger particles produces unrealistically low apparent densities. Interestingly, the relationship between modeled and SPM method densities is not linear (Figure 3.4). Two hypotheses can explain the nonlinear relationship between density estimates. The first relates to particle packing. Large particles with lower density may have fractal

dimensions that are less than 2, indicating that the particles are more porous than assumed [*Nikora et al*., 2004; *Hill et al*., 2011]. The second hypothesis is that when particles are large and density is low, the component particles of the larger flocs may have higher organic contents, and when particles are small and density is large, the component particles may have higher inorganic contents [*Babin et al.*, 2003; *Hill et al.*, 2013]. Although the model does an adequate job of predicting density overall, it does not resolve details of the relationships among component particle composition, particle packing geometry in flocs, and apparent density. These deficiencies can be addressed by the methods presented here.

4.4 Time Series

Based on the correlation between the SPM method apparent density and apparent densities estimated with the LD method, it is reasonable to use time series of particle size distributions and beam attenuation to construct time series of proxies for apparent density (Figures 4.2 and 4.3). The non-linear relationship between the model estimates of apparent density and the SPM method apparent density means that the model will tend to overestimate apparent density when densities are low and underestimate apparent density when densities are high. Nonetheless, time series of the proxies can yield insight into particle dynamics in the bottom boundary layer.

In addition to densities estimated with the LD method, another estimate of density is based on LISST data alone:

$$\rho_a = \frac{M_{Cp}}{V_{LISST}} \qquad [22]$$

The above is equivalent to Equation 11 except V_t is replaced with V_{LISST}, which is the volume estimated from the LISST only. This apparent density proxy is included in the time series analysis because the LISST is a commercially available, widely used instrument. While it is more accurate to merge LISST and DFC data to span the entire size distribution, the DFC it is a custom instrument. Therefore, densities calculated using just LISST data are a more widely accessible proxy for apparent density. In the time series, M_{cp} is calculated by dividing c_p by the c_p*:SPM* ratio measured during the

experiments. For reference, time series of c_p:V_{LISST} are presented as well (Figures 4.2 and 4.3).

Time series from Oasis 2007 and Hudson both have large dynamic ranges in apparent density, and densities respond differently to forcing in the two experiments. For Oasis 2007, shear velocity measurements were made by colleagues at Woods Hole Oceanographic Institution [see *Hill et al.*, 2011], while the shear velocity measurements from the Hudson were made by colleagues at the Bedford Institute of Oceanography [unpublished].

In Oasis 2007 (Figure 4.2), around year day 255 and again around year day 258, increases in beam attenuation lagged increases in shear velocity. Beam attenuation increased after the peak in shear velocity. The lag likely arose because there was a limited supply of resuspendable sediment in the seabed. As shear velocity increased the limited supply of sediment was resuspended and distributed throughout a thick boundary layer, which resulted in lower beam attenuation, initially. As the stress began to decrease, the boundary thinned. Sediment sank into this thinner boundary layer but did not deposit immediately because stresses were too high. The net flux of sediment into a thinner boundary layer caused sediment concentration and beam attenuation to increase. Accompanying the increase in beam attenuation was a decrease in apparent density. A decrease would have occurred if flocculation rate increased in response to larger concentrations, which would have produced larger flocs with lower apparent densities. Eventually when stress was low enough, large flocs deposited, leaving only

small, relatively dense microflocs and single grains in suspension. These particles had larger apparent densities.

In the Hudson (Figure 4.3) experiment, two peaks in beam attenuation and in apparent density are observed daily. The peaks occur at low tide slack water. Small increases in beam attenuation occur at high water. Shear velocities fall to much lower values at low slack water than they do at high water. The increase in beam attenuation is a result of the thin bottom boundary layer, much like the observation with Oasis 2007. When shear velocity is nearly 0, beam attenuation and apparent density increases. Although there is an overall increase in beam attenuation, there is a relative decrease in beam attenuation when there is a peak in apparent density (Figure 4.3). This result is likely due to larger flocs settling out of suspension, leaving only denser small flocs and single grains suspended in the bottom boundary layer. Larger flocs are less dense then sediment grains but deposit faster because they are larger. When shear velocity increases from 0, recently deposited flocs get resuspended, resulting in increased beam attenuation. This increase in beam attenuation can also be observed as shear velocity approaches 0. During high tide, beam attenuation is low, apparent density is low and shear velocity is high. At this time the bottom boundary layer increases in thickness, resulting in lower suspended sediment concentrations. The larger bottom boundary layer dilutes the sediment concentration, which explains the lows in beam attenuation and apparent density. On June 8th, 2013 (approximately year day 159), a major rainfall event occurred in the Minas Basin [*Environment Canada*, 2013]. After this event, peaks in beam attenuation are relatively higher than earlier in the experiment. Conversely,

peaks in apparent density are relatively lower. This suggests that after the rainfall event, more sediment was available, which resulted in more rapid flocculation. The post rainfall event flocs are larger and relatively less dense, which explains the relative increase in beam attenuation peaks and relative decrease in apparent density peaks.

Apparent density proxies are important as they provide information on flocculation and clearance rate. This has been demonstrated in the time series analysis where two different trends in apparent density are observed with an increase in beam attenuation. In the Oasis 2007 experiment apparent density decreases when beam attenuation increases. This indicates that when sediment concentrations were high, the sediment in suspension was composed mostly of large, low-density flocs. In the Hudson experiment, apparent density increases when beam attenuation increases. This indicates that when sediment concentration was high, the sediment in suspension was composed mostly of single sediment grains and small flocs with higher density. After a significant rainfall event, the increases in apparent density are relatively lower when compared to the increases earlier in the experiment. This implies that sediment was more available after the event, which initiated flocculation. This allowed larger lower density flocs to be introduced into the suspension.

The use of apparent density proxies provides vital information on particle properties and flocculation in the bottom boundary layer. This has been demonstrated by comparing two time series analysis from two different aquatic environments.

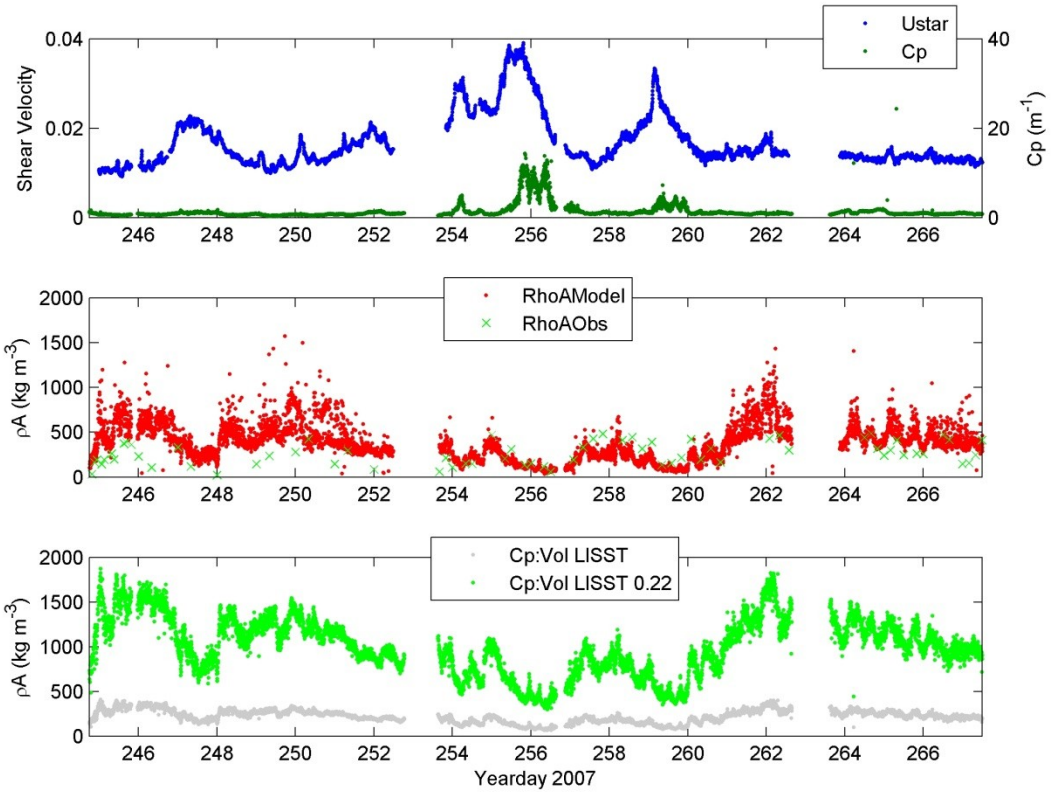

Figure 4.2: Time series analysis for Oasis 2007. The top panel contains time series of shear velocity in blue (cm s^{-1}) and beam attenuation in green (c_p, m^{-1}). The middle panel contains model density in red (kg m^{-3}) and SPM method density in green (kg m^{-3}). The bottom panel contains apparent density using LISST data in grey (kg m^{-3}) and apparent density using LISST data with a c_p*:SPM* ratio from *Hill et al.* [2011] in green (kg m^{-3}).

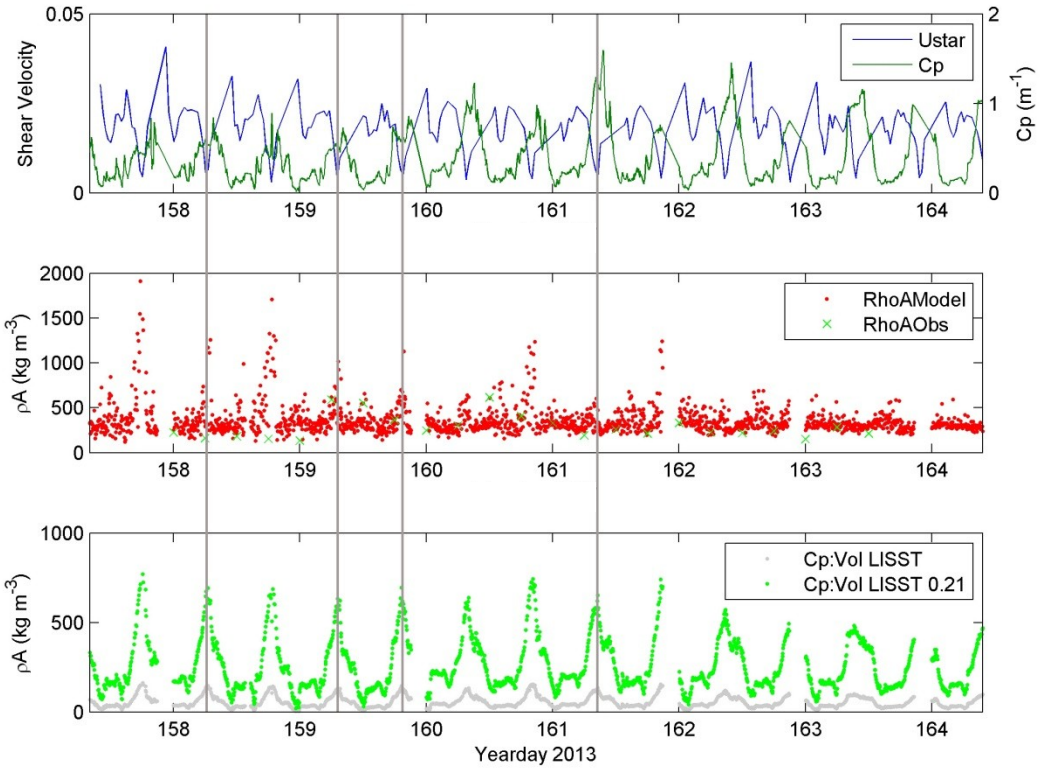

Figure 4.3: Time series analysis for the HUDSON experiment. The x-axis represents the yearday sample times during 2013. The grey vertical lines mark representative times of low tide slack water. This times were with respect to the significant rainfall event. The top panel contains time series of shear velocity in blue (cm s^{-1}) and beam attenuation in green (c_p, m^{-1}). The middle panel contains model density in red (kg m^{-3}) and SPM method density in green (kg m^{-3}). The bottom panel contains apparent density using LISST data in grey (kg m^{-3}) and apparent density using LISST data with a c_p*:SPM* ratio calculated from using the method outlined by *Hill et al.* [2011] in green.

Chapter 5.0 - Future Work

5.1 Camera Development

Although the apparent densities estimated using the DVC method do not correlate well with those estimated using the LD method, the data collected using the DVC are useful for generating a density model for particles smaller than the lower limit of resolution of the camera. The most likely hypothesis for the poor comparison between the DVC method and LD method is related to the particle size restrictions of the camera used in the DVC method. DVC sample intervals can have a significantly large range (e.g. one sample every hour), and thus the video camera may not experience all events during a deployment. This is important when comparing the DVC method estimates in time series with the LD method.

Given the restrictions of the video camera, emphasis should be placed on the development of a new camera that is capable of sampling smaller particles more frequently. With a video camera that is capable of imaging particles smaller than the current camera, a comparison between the DVC method and the LD method should reveal better correlation between the two estimates of density. If data from a new video camera correlated with the LD method, then the LD method can be further validated as an accurate replacement. This validation is necessary because although the SPM method and LD method are correlated, the same particle volume concentration is used in both methods. The DVC method uses measurements independent of the LD method, therefore this analysis using a camera with higher resolution would provide

further evidence that the LD method is an accurate proxy for apparent density. In addition to this, higher camera resolution would also be useful for creating a more accurate model of apparent density as a function of particle size. Finally, higher resolution time series would make it possible to observe the differences in size versus settling velocity during high stress and low stress events.

5.2 Laboratory Study

Controlled laboratory studies for comparing the various estimates of apparent density would assist in proving or disproving the correlation between the DVC and LD method. Different variables could be manipulated, such as the effect of Coloured Dissolved Organic Matter (CDOM) on collected data, the use of artificial particles with known size and density, and different particle populations with different refractive indices. Results from these controlled laboratory studies would reveal whether there are any systematic biases in the methods presented.

5.3 Particle Composition

A limitation of this study is that particle composition has not been considered when estimating apparent density. Although the results are promising, it is important to consider how particle composition affects SPM, and more specifically the c_p:SPM ratio. The c_p:SPM ratio is a function of composition and a viable measurement that does account for particle composition is backscatter ratio [*Twardowski et al.*, 2001]. When backscatter ratio is high, the flocs are composed mostly of inorganic particles, and when backscatter ratio is low the flocs are mostly composed of organic particles. If particle

composition were considered, then variance in the relationship between the optical proxy for density and density from the SPM method could be reduced [*Babin et al.*, 2003; *Hill et al.*, 2013].

Chapter 6.0 - Conclusion

6.1 Conclusion

In conclusion, the apparent densities estimated using LD method are linearly correlated with those estimated using the SPM method. This result is significant because it suggests that the LD method could be used as an accurate proxy for apparent density. However, the apparent density estimates using the LD method do not correlate with the independent density estimates from the DVC method. Lack of correlation is due to the relatively larger lower limit resolution of the DVC. In an attempt to correct for this, a model [*Maggi*, 2013] was applied to newly collected and archived DVC data to predict particle densities for the entire size distribution. While the model does an adequate job of predicting densities, the relationship between modeled and the SPM method densities is not linear. The exponential relationship between the model and the SPM method apparent densities likely arises due to the model overestimating density at lower SPM method densities and underestimating density at higher SPM method densities. This result was likely due to the model assuming a fractal dimension of 2. If fractal dimensions were less than 2 for low density flocs, this would result in over estimates in the model.

Trends in apparent density compared with trends in shear velocity and beam attenuation can be used to interpret which processes affect particle properties in the bottom boundary layer. In the Oasis 2007 time series, the offset between beam attenuation and shear velocity likely occurs because there was a limited sediment

supply that was suspended throughout a thick boundary layer when shear velocity increased. As shear velocity decreased, the bottom boundary layer collapsed, allowing sediment deposition into the thin boundary layer, which resulted in higher sediment concentrations. The lag between beam attenuation and apparent density is interpreted as an increase in flocculation due to the high sediment concentrations. When the large flocs are in suspension, apparent density is low. When the large flocs are deposited, apparent density increased. Observations in the Hudson experiment provides information on flocculation in a tidally dominated environment. Early in the Hudson experiment, peaks in beam attenuation and apparent density (when shear velocity is approximately 0) suggest that single sediment grains and small flocs remained in suspension while larger flocs deposited due to their size. Early in the experiment, sediment availability was limited and flocculation did not occur. After a significant rainfall event mid experiment, peaks in beam attenuation were relatively larger compared with peaks earlier in the experiment. Peaks in apparent density were relatively smaller after this event. These observations suggest that the rainfall event facilitated flocculation.

Ultimately, development of a new DVC that has the ability to resolve smaller particles would provide more insight into whether the LD method is a suitable replacement for the DVC method. Based on the promising results that are presented here, the LD method is a suitable replacement for the SPM method. However, because the variable estimates used in the DVC method are independent of those used in the LD

method, correlation between these methods would further validate the LD method as an accurate proxy for apparent density.

References

Agrawal, Y.C. and H.C. Pottsmith (2000), Instruments for particle size and settling velocity observations in sediment transport, *Marine Geology*, *168*, 89-114.

Babin, M., A. Morel, V. Fournier-Sicre, F. Fell, and D. Stramski (2003), Light scattering properties of marine particles in coastal and open ocean waters as related to the particle mass concentration, *Limnology and Oceanography*, *48*, 843-859.

Boss, E., L. Taylor, S. Gilbert, K. Gundersen, N. Hawley, C. Janzen, T. Johengen, H. Purcell, C. Robertson, D.W.H. Schar, G.J. Smith, and M.N. Tamburri (2009), Comparison of inherent optical properties as a surrogate for particulate matter concentration in coastal waters, *Limnology and Oceanography: Methods*, *7*, 803-810.

Curran, K.J., P.S. Hill, T.G. Milligan, O.A. Mikkelsen, B.A. Law, X. Durrieu de Madron, and F. Bourrin (2007), Settling velocity, effective density, and mass composition of suspended sediment in a coastal bottom boundary layer, Gulf of Lions, France, *Continental Shelf Research*, *27*, 1408-1421.

Downing, J. (2006), Twenty-five years with OBS sensors: The good, the bad, and the ugly, *Continental Shelf Research*, *26(17-18)*, 2299-2318.

Environment Canada (2013), Canadian Climate Data, Retrieved from http://climate.weather.gc.ca/climateData/dailydata_e.html?timeframe=2&Prov=NS%20%20&StationID=27141&dlyRange=1996-07-01|2015-03-29&Year=2013&Month=6&Day=29 on March 30, 2014.

Fennessy, M.J., K.R. Dyer, and D.A. Huntley (1994), INSSEV: An instrument to measure the size and settling velocity of flocs in situ, *Marine Geology*, *117(1-4)*, 107-117.

Fennessy, M.J., and K.R. Dyer (1996), Floc Population Characteristics Measured With INSSEV During The Elbe Estuary Intercalibration Experiment, *Journal of Sea Research*, *36(1/2)*, 55-62.

Fox, J.M., P.S. Hill, T.G. Milligan, A.S. Ogston, and A. Boldrin (2004), Floc fraction in the waters of the Po River Delta, *Continental Shelf Research*, *24*, 1699-1715.

Hill, P.S., J.P. Syvitski, E.A. Cowan, and R.D. Powell (1998), In situ observations of floc settling velocities in Glacier Bay, Alaska, *Marine Geology, 145(1-2),* 85-94.

Hill, P.S., E. Boss, J.P. Newgard, B.A. Law, and T.G. Milligan (2011), Observations of the sensitivity of beam attenuation to particle size in a coastal bottom boundary layer, *Journal of Geophysical Research, 116,* C02023, 1-14.

Hill, P.S., D.G. Bowers, K.M. Braithwaite (2013), The effect of suspended particle composition on particle area-to-mass ratios in coastal waters, *Methods in Oceanography*, *7*, 95-109.

Khelifa, A., and P.S. Hill (2006), Models for effective density and settling velocity of flocs, *Journal of Hydraulic Research*, *44(3),* 390-401.

Maggi, F. (2013), The settling velocity of mineral, biomineral, and biological particles and aggregates in water, *Journal of Geophysical Research: Oceans*, *118*, 2118-2131.

McCave, I.N. (1984), Size spectra and aggregation of particles in the deep ocean, *Deep Sea Research*, *Part A*, *31(4)*, 329-352.

Mikkelsen, O.A., and M. Pejrup (2000), In situ particle size spectra and density of particle aggregates in a dredging plume, *Marine Geology*, *170*, 443-459.

Mikkelsen, O.A., and M. Pejrup (2001), The use of a LISST-100 laser particle sizer for in-situ estimates of floc size, density and settling velocity, *Geo-Marine Letters*, *20*, 187-195.

Mikkelsen, O. A., T.G. Milligan, P.S. Hill, and D. Moffatt (2004), INNSECT - An instrumented platform for investigating floc properties close to the seabed, *Limnology and Oceanography-Methods, 2*, 226-236.

Mikkelsen, O.A., T.G. Milligan, P.S. Hill, and R.J. Chant (2005), In situ particle size distributions and volume concentrations from a LISST-100 laser particle sizer and a digital floc camera, *Continental Shelf Research*, *25(16)*, 1959-1978.

Neukermans, G., H. Loisel, X. Meriaux, R. Astoreca, and D. McKee (2012), In situ variability of mass-specific beam attenuation and backscattering of marine particles with respect to particle size, density, and composition (2012), *Limnology and Oceanography*, *57(1)*, 124-144.

Nikora, V., J. Aberle, and M.Green (2004), Sediment flocs: Settling velocity, flocculation factor, and optical backscatter, *Journal of Hydraulic Engineering*, *130(10)*, 1043-1047.

Otsu, N. (1979), A threshold selection method from gray-level histograms, *IEEE Trans. Syst. Man Cybern.*, *9(1)*, 62-66.

Ogston, A.S., and R.W. Sternberg (1999), Sediment-transport events on the northern California continental shelf, *Marine Geology*, *154*, 69-82.

Rubey, W.W. (1933), Settling velocities of gravels, sand, and silt particles, *American Journal of Science*, *25(148)*, 325-338.

Sternberg, R.W., I. Berhane, and A.S. Ogston (1999), Measurement of size and settling velocity of suspended aggregates on the northern California continental shelf, *Marine Geology*, *154*, 43-53.

Snyder, W.A., R.A. Arnone, C.O. Davis, W. Goode, R.W. Gould, S. Ladner, G. Lamela, W.J. Rhea, R. Stavn, M. Sydor, and A. Weidemann (2008), Optical scattering and backscattering by organic and inorganic particulates in the U.S. coastal waters, *Applied Optics*, *47(5)*, 666-677.

Twardowski, M.S., E. Boss, J.B. Macdonald, W.S. Pegau, A.H. Barnard, J. Ronald, and V. Zaneveld (2001), A model for estimating bulk refractive index from the optical backscattering ratio and the implications for understanding particle composition in case I and case II waters, *Journal of Geophysical Research*, *106*, 14129-14142.

Winterwerp, J.C., and W.G.M. van Kesteren (2004), Introduction to the physics of cohesive sediment in the marine environment, *Developments in Sedimentology*, *56*, 466.

Appendix

The supplementary data files mentioned in the thesis are available on DalSpace.